> JSTARS-2023-00194 <

Observation and assessment of model retrievals of surface exchange components over a row canopy using directional thermal data

Mwangi S., G. Boulet, M. LePage, J-P. Gastellu-Etchegorry, J. Bellvert, B. Lemaire, P. Fanise, J-L. Roujean, and A. Olioso

***Abstract*—Land surface temperature is an essential climate variable that can serve as a proxy for detecting water deficiencies in croplands and wooded areas. Its measurement can however be influenced by anisotropic properties of surface targets leading to occurrence of directional effects on the signal. This may lead to an incorrect interpretation of thermal measurements. In this study, we perform model assessments and check the influence of thermal radiation directionality using data over a vineyard. To derive the overall directional surface temperatures, elemental values measured by individual cameras were aggregated according to the respective cover fractions/weights in viewing direction. Aggregated temperatures from the turbid model were compared to corresponding temperatures simulated by the 3D DART radiative transfer model. The reconstructed temperatures were then used in surface-energy-balance (SEB) simulations to assess the impact of the Sun-target-sensor geometry on retrievals. Here, the pseudo-isotropic Soil-Plant-Atmosphere-Remote-Sensing-of-Evapotranspiration (SPARSE) dual-source model together with the non-isotropic version (SPARSE4), were used. Both schemes were able to retrieve overall fluxes satisfactorily, confirming a previous study. However, the sensitivity (of flux and component temperature estimates) of the schemes to viewing direction was tested for the first time using reconstructed sets of directional thermal data to force the models. Degradation (relative to nadir) in flux retrieval cross-row was observed, with better consistency along rows. Overall, it was nevertheless shown that SPARSE4 is less influenced by the viewing direction of the temperature than SPARSE, particularly for strongly off-nadir viewing. Some directional/asymmetrical artefacts are however not well reproduced by the simple Radiative Transfer Methods (RTM), which can then manifest in and influence the subsequent thermal-infrared-driven SEB modelling.**

***Index Terms*—evapotranspiration, surface-energy-balance, temperature-inversion, thermal-radiation-directionality, vineyard**

I. INTRODUCTION

THE economic livelihood of many semi-arid regions largely depends on fruit production. Vineyards, for example, are commonplace in the relatively dry or semiarid regions of Spain. With evapotranspiration (ET, which includes other consumptive water use, *inter alia*, by animals/humans, from open water bodies) accounting for nearly all the water used from such areas [1], accurate ET retrieval methods are necessary to optimise irrigation water demand. This can be achieved by solving the soil water balance [upto the rootzone] with the aim of quantifying soil water deficits that indicate the need for supplementary irrigation and better provide for the climatic demand. Methods that directly estimate states in the vadose zone however require input variables that are difficult to estimate, and whose uncertainties may lead to poor estimates of water needs. Alternatively, indirect methods that use proxies to establish water-status can be used. In this regard, several methods have been proposed, with some already operational, including physically-based surface energy balance (SEB) methods (e.g. SEBS [2]; SEBAL [3]; TSEB [4]). Typically, terrestrial variables related to water availability are required to drive these models, i.e. to set the boundary conditions for near land surface interactions. For instance, remote sensing based methods use the land surface temperature (LST) as a proxy for water status when inverting the surface energy budget for ET estimates. As such, LST can also act as a key descriptor in drought and water stress indices [5], [6]. LST is typically derived from the emission signals observed by radiometers sensing in the thermal infrared spectral domain.

Compared to in-situ thermal measurements, remotely sensed surface temperatures allow the monitoring of water fluxes over larger spatial scales. However, several issues arise when using

This paragraph of the first footnote will contain the date on which you submitted your paper for review, which is populated by IEEE. It is IEEE style to display support information, including sponsor and financial support acknowledgment, here and not in an acknowledgment section at the end of the article. For example, "This work was supported in part by the U.S. Department of Commerce under Grant 123456." The name of the corresponding author appears after the financial information, e.g. *(Corresponding author: Second B. Author).* Here you may also indicate if authors contributed equally or if there are co-first authors.

The next few paragraphs should contain the authors' current affiliations, including current address and e-mail. For example, First A. Author is with the National Institute of Standards and Technology, Boulder, CO 80305 USA (e-mail: author@ boulder.nist.gov).

Second B. Author Jr. was with Rice University, Houston, TX 77005 USA. He is now with the Department of Physics, Colorado State University, Fort Collins, CO 80523 USA (e-mail: author@lamar.colostate.edu).

Third C. Author is with the Electrical Engineering Department, University of Colorado, Boulder, CO 80309 USA, on leave from the National Research Institute for Metals, Tsukuba 305-0047, Japan (e-mail: author@nrim.go.jp).

Mentions of supplemental materials and animal/human rights statements can be included here.

Color versions of one or more of the figures in this article are available online at http://ieeexplore.ieee.org

thermal data from satellite sensors: missing data (for example, due to overcast conditions), inadequate spatial and temporal resolutions, and thermal radiation directionality (TRD) issues. Efforts have mostly been directed towards addressing the first two, for example, by applying gap filling methods, data fusion techniques, proposing missions with improved revisit times and spatial resolutions, applying disaggregation techniques, among others. Limited focus has however been placed on analysing/evaluating how thermal directionality influences flux retrieval although many TRD models have been proposed [7], [8]. In recent literature, [9] have for instance proposed a framework for correcting angular effects that could help improve flux retrieval in single-source SEB methods. Granted, [10] have postulated that the contribution of surface temperature uncertainties to errors in the estimation of the energy balance could rank lower relative to uncertainty in other variables required in SEB schemes; notably, the uncertainty in wind speed and the roughness lengths for turbulent flux exchange. Nonetheless, uncertainties due to thermal directionality, which can lead to large nadir-off nadir differences; for instance, up to 15 K were observed over vineyards [11], and this can lead to inaccuracies in retrieved turbulent fluxes. Additionally, since the relationship between the roughness lengths of heat (which is influenced by the thermal dynamic state of the surface [2]) and momentum - where they help distinguish between aerodynamic and radiant temperatures [12], [13] through their contribution to the aerodynamic resistance - any errors arising from an insufficient roughness length parameterization can, by extension, be attributed to uncertainties in temperature. This necessitates the use of realistic surface temperatures when estimating the energy balance.

Vineyards represent complex heterogeneous canopies for heat exchange due to the strong contrast between the soil (inter-row) and the vegetation. Such complex and contrasting remote sensing targets induce considerable directional variability on the observed surface signals depending on the sensor's view direction [14]. For instance, cross-row, the gap (or soil) fraction (and thus the observed soil emissions) will vary considerably with viewing zenith/elevation since the further from nadir, the larger the fraction of vegetation in view. This is however not the case when observing along the row where the gap fraction exhibits little variation with viewing elevation. Additionally, depending on the row orientation, the proportion of the viewed gap that is illuminated or shaded will change depending on the time or position of the sun. The direction of the sun (relative to the row geometry, whether along- or cross row) will also influence the radiation intercepted and consequently retained by the various surface components.

The aim of the current study was to analyse the relationship between surface energy balance components (including latent heat/evapotranspiration) and the directional LST in a row canopy. Specifically: *i)* the analysis of energy budget components measured over a row canopy, *ii)* modeling and assessment of directional temperatures and surface exchange components using radiative transfer and SEB schemes, respectively; *iii)* applying the directional thermal data so as to analyze and evaluate the consistency of flux retrieval in a row canopy. To this end, a field campaign within the framework of the HiLiaise, CNES/TRISHNA [15] and ESA WineEO projects was conducted during the spring and summer periods of 2021 in a Tempranillo vineyard located in Lleida province, north-eastern Spain. In addition to meteorological and elemental temperature measurements, various components of the radiation and surface energy balance were monitored. After performing initial corrections aimed at enhancing the observed surface energy budget, the data were applied in model evaluations. Land surface temperature is required as an input variable for inference of the prevailing terrestrial water status. This proxy was reconstructed from the elemental thermal measurements, consequently allowing the evaluation/comparison of retrievals from relatively simple radiative transfer methods with those simulated by a more realistic and comprehensive 3-D model. Regarding the near-land surface processes, the Soil Plant Atmosphere Remote Sensing of Evapotranspiration (SPARSE and SPARSE4) simulated the energy exchanges during the period. Meteorological, biophysical and reconstructed temperature data were used to drive the SPARSE and SPARSE4 formulations. In the following, the site along with the collected and processed data are described. The results from the model assessments are then presented.

II. Materials and Methods

This section begins by describing the experimental site and the instruments installed therein. The following sub-section briefly summarizes the different methods applied in this study. Finally, details on the data collected during the field campaign are given including: what data were measured; procedures undertaken for the energy budget closure corrections; and directional temperature reconstructions.

A. Site description and instrumentation

The study area is located in Verdu, Lleida province, north-east of Spain (latitude: 41.596° N; longitude: 1.126° E). The vineyard at the site is privately owned and managed. Lleida has a temperate semi-arid climate (class BSk, Koppen climate classification) characterised by cold winters and hot dry summers, with the annual potential evapotranspiration often exceeding the precipitation. The cultivar (grape variety) is Tempranillo. The tree spacing is ~1.1 m and the row spacing ~4.1 m with the vineyard's rows oriented roughly East-West (~110° from north). The row scene schematic is shown in **Figure 1**. The vineyard was drip irrigated with drippers spaced 0.6 m apart along a single drip line per vine row. Irrigation scheduling was conducted according to the FAO-56 Penman-Monteith method. The land use of the immediate vicinity is predominantly viticultural. According to results of a soil analysis of the site, the sand, loam, clay compositions are 26.32%, 28.36%, 45.32%, respectively. The soil's relatively stony nature, especially at the topmost layer, helps to control and thus reduce evaporation losses allowing more effective

irrigation water usage.

Instrumentation

The data collection campaign took place from April to September 2021. The experimental installations (instruments) at the study site included:

- SN 500-SS four-component net radiometer (Apogee Instruments) for observing down- and up-welling shortwave (model SP-510 and model SP-610, respectively) and longwave (model SL-510 and SL-610, respectively) radiation fluxes. Due to logistical constraints, the instrument was installed atop the row/canopy hence mostly viewing the vegetation elements.
- An eddy covariance system (IRGASON instrument, Campbell Scientific) for the monitoring of turbulent flux exchanges installed 3 m above the ground surface. It combines an open-path gas analyzer with a 3D sonic anemometer.

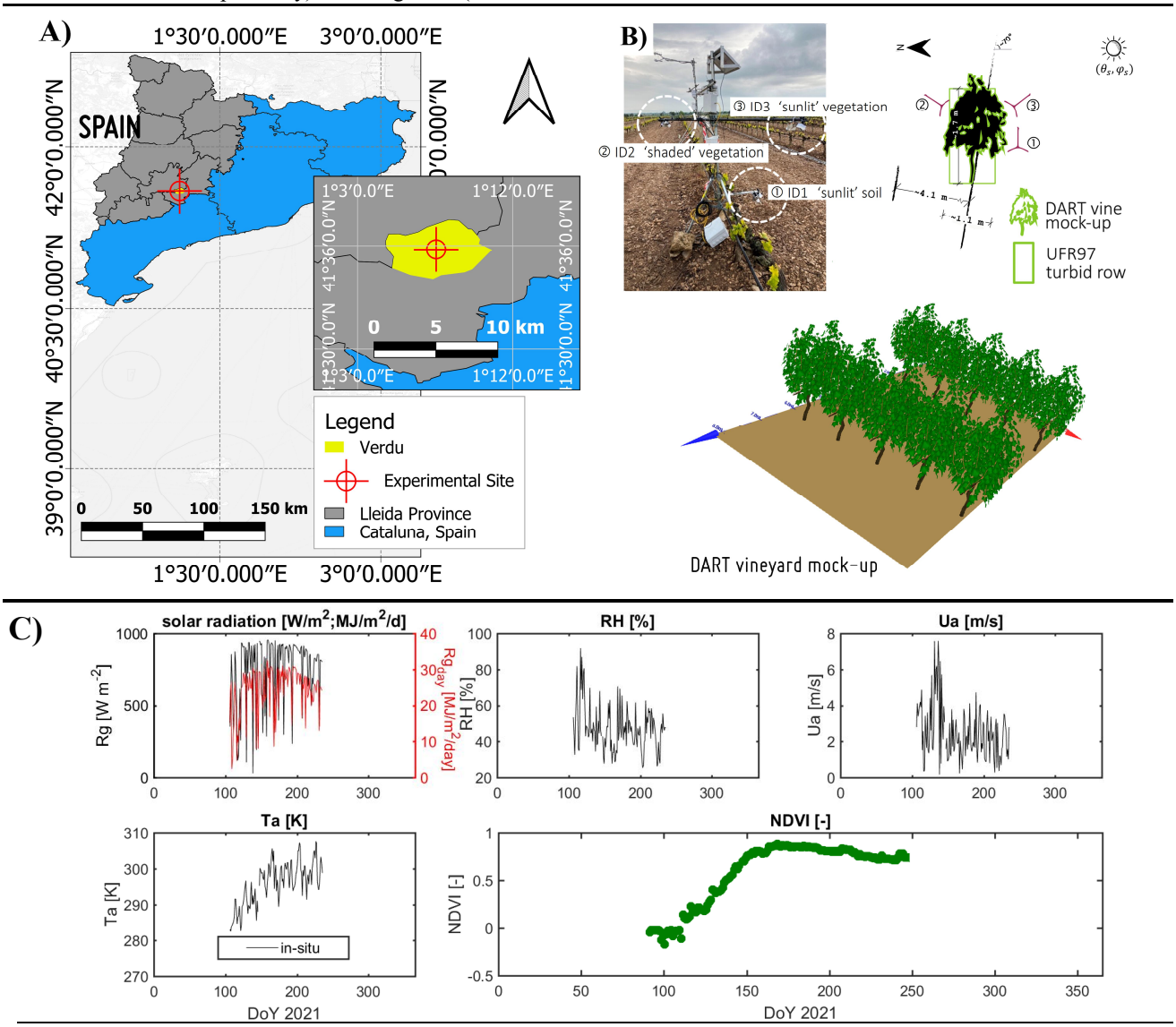

Figure 1: **A)** Map of the experimental study site in Verdu, Cataluña, Spain (adapted from data retrieved from gadm.org). **B)** The eddy covariance system and thermal camera installations at the vineyard; and a depiction of the scene & setup details. **C)** The [noon] meteorological and other variables – in-situ observations at the Verdu experimental site, and the NDVI computed using the near infrared and red signals measured above the canopy

- Hygrovue5 temperature and humidity sensor (Campbell Scientific) for measuring the air temperature and relative humidity above the canopy at ~3 m.
- Three HFP01 soil conduction plates placed at 5 cm depth below the surface for sensing the ground heat flux. Two of the plates were placed under the canopy and one between the rows. Subsequent correction to include the heat storage at the top layer was done using the calorimetric method (described further below).
- Thetaprobes (DeltaT ML2x) for soil moisture and

soil temperature measurements. Three probes were installed under the canopy sensing at varying depths (5, 15, 30 cm) and one installed between the rows at 5 cm depth.

- Three SKR 1840 NDVImetre sensors (SKYE Instruments) for observing the irradiance and radiances in the red and near infrared spectral domains. That is, one NDVI (Normalized Difference Vegetation Index) instrument observed the respective narrow-band irradiances while the other two were placed such that they could observe the radiances atop the canopy and bare soil, respectively.
- Thermal MLX90641 IR cameras (ID1, ID2, ID3) for measurement of the component surface temperatures (i.e., sunlit soil, shaded and sunlit vegetation, respectively). The TIR cameras have 16x12 pixels (with a field of view of X direction: 110°; Y direction: 75°), and have an accuracy of ~±1.5 °C (under isothermal conditions). These were installed to view the bare soil, and the vegetation from two directions (i.e., in the sun's direction and in the shade) and sampling every 15 minutes. To be consistent with most of the other observed variables (with 30-minute acquisition intervals), only the half hourly temperatures were used. See **Figure 1** for the installation set-up.

Selected radiation and meteorological variables are displayed in **Figure 1**.

B. Methods

Here we briefly summarize the various methods used within this study. These include: radiative transfer models that describe the interaction of radiation fluxes within the surface/canopy; and surface energy balance schemes that estimate energy exchanges at the near-land surface (where radiative transfer and energy budget modules are combined for radiation and turbulent fluxes estimation/partitioning, respectively).

Radiative transfer models

The Unified François radiative transfer method [16] extends [17] by incorporating BRDF (bidirectional reflectance distribution function) and row canopy aspects proposed in [18]. The row crop gap frequency formulation in [18] basically splits the scene into two, *i)* gaps between the rows, with a gap probability of 1 when viewed at parallel projection from nadir, and *ii)* the vegetated row, where the gap fraction is calculated using a Beer-Lambert approximation following [19].

DART (discrete anisotropic radiative transfer [20]) is a comprehensive radiative transfer scheme that simulates the remote sensing images and 3D radiative budget of natural and urban landscapes, from the visible to the thermal infrared spectral domains. It can simulate leaf specular, polarization and sun induced fluorescence mechanisms as well as topography and the hotspot [20], for any instrumental and experimental configuration.

4SAIL (the thermal-based four-stream scattering by arbitrarily inclined leaves [21]) is a 1D thermal radiative transfer model that does not account for canopy heterogeneity.

Surface energy balance

In this study, we apply the Soil Plant Atmosphere Remote Sensing of Evapotranspiration (SPARSE, [22]) model to simulate the land surface energy exchanges. SPARSE, like the two source energy balance model TSEB [4], is a surface energy balance (SEB) method that simulates soil-vegetation-atmosphere interactions and consequently retrieves actual/prevailing surface (soil and vegetation) energy fluxes by inverting the surface temperature. The scheme was recently extended (named SPARSE4) to discriminate the soil and vegetation sources into their respective sunlit/shaded components [23] where an extended energy balance scheme was coupled with the aforementioned Unified François radiative model [16], [18]. The algorithms' overall surface energy budget expressions are identical to Equation (3) (which is used in the observed energy imbalance corrections) with the partitioning of the available energy between the various components written as;

$$(R_n - G) - (H + \lambda E) = \sum_{xx} R_{n,xx}(1- \xi) - (H_{xx} + \lambda E_{xx}) = 0 (1)$$

where R_n [W m^{-2}] is the net radiation, G [W m^{-2}] is the ground heat flux, ξ is the fraction of soil/ground heat net radiation stored in the soil substrate, i.e., $\xi = G/R_{ng}$. Accordingly, it is set to 0 for vegetation elements. λE [W m^{-2}] and H [W m^{-2}] are the latent heat and sensible heat fluxes, respectively. In the definition (thus partitioning) of the different radiation and turbulent fluxes, $xx = v, g$ and $xx = vs, vh, gs, gh$ for SPARSE and SPARSE4, respectively.

The schemes employ a Penman-Monteith approximation method to estimate the latent heat flux with aerodynamic resistances for heat and momentum exchanges formulated following [24]. Similar to the Surface Energy Balance System SEBS [2], potential and fully stressed limits are set for physically-consistent flux estimates. To simulate the water status as characterised by the surface boundary condition (i.e., surface temperature, which can help describe the conditions at the aerodynamic level), it is assumed that the soil will be stressed before the vegetation; for this, evaporation and transpiration efficiency terms are introduced. As such, the system starts with the respective soil and vegetation components evaporating and transpiring at potential rates, with the evaporation efficiency of the soil reduced first (until soil water is depleted, i.e., at minimum soil efficiency) followed by that of the vegetation until convergence.

C. Data, data processing procedures and methodology

Biophysical data

The leaf area index (LAI) was measured using a destructive approach. Since the canopy cover is expected to vary during vine development, it was necessary to scale the LAI so as to ensure a temporal trend. An exponential regression (following the NDVImeter documentation, e.g. Equation (2) [25]) was hence fitted. To this end, the red and near infrared (NIR)

radiation signals measured by the NDVImeter sensors were used to compute the normalized difference vegetation index as:

$$\mathrm{NDVI} = \frac{\rho_{\mathrm{NIR}} - \rho_{\mathrm{RED}}}{\rho_{\mathrm{NIR}} + \rho_{\mathrm{RED}}};\ \mathrm{LAI} = \mathrm{a} \cdot \mathrm{e}^{(\mathrm{bNDVI})} \qquad (2)$$

where $\rho = \mathrm{radiance/irradiance}$ is the reflectance in the near infrared (NIR) and RED spectral domains. The derived NDVI (from radiation signals acquired above the canopy, **Figure 1**C) were subsequently used to scale the clumped LAI to mimic the vegetative growth throughout the period. The temporally varying canopy cover obtained from this procedure was applied in other parts of this study, i.e., for the energy balance closure corrections and in the modelling exercises.

Processing and correction of the raw eddy covariance data was carried out using the *EasyFlux DL* (Campbell Scientific) program. A simple gap-filling method (linear interpolation - based on the instantaneous to daily flux ratio from the immediate observed past) was then applied to address any missing data in the processed turbulent fluxes. The simplified gap-filling method was warranted as only a few gap instances presented in the measurements. Regardless, in EB/EC correction studies with many missing data that may lead to insufficient and thus incorrect interpretations, comprehensive methods (such as the physically-based full-factorial gap-filling scheme proposed in [26]) should be preferred. The wind speed ($\mathrm{u_a}$) was recomputed from the horizontal wind speed vector components from the sonic anemometer, i.e., $\mathrm{u_a} = (\mathrm{u}^2 + \mathrm{v}^2)^{0.5}$.

Available energy, turbulent fluxes and the energy balance closure

The total available energy at the surface ($\mathrm{R_n} - \mathrm{G_0}$) is used up for the turbulent energy exchanges (sensible and latent heat fluxes). This yields the surface energy balance equation commonly written as:

$$\mathrm{R_n} - \mathrm{G_0} = \lambda\mathrm{E} + \mathrm{H} \qquad (3)$$

where all terms are as previously defined, i.e., $\mathrm{R_n}$ [$\mathrm{W\,m^{-2}}$] the overall net radiation equivalent to total (solar and thermal) irradiances less total radiances, $\mathrm{G_0}$ [$\mathrm{W\,m^{-2}}$] is the ground heat flux in the soil column, $\lambda\mathrm{E}$ [$\mathrm{W\,m^{-2}}$] and H [$\mathrm{W\,m^{-2}}$] are the latent heat energy and sensible heat energy fluxes, respectively.

Unlike other methods (for example, flux variance, surface renewal) that can only measure surface turbulent fluxes indirectly, eddy covariance (EC) systems allow direct measurement of latent and sensible fluxes [27]–[29]. As a result, the ideal energy budget closure, where the observed available energy is equivalent to the measured turbulent fluxes, is rarely achieved in EC. The observed available energy has, in most cases, been found to be larger than the observed turbulent fluxes [30]. This is the well documented energy balance closure problem, which has been investigated and shown to be a recurring issue in multitudes of flux experimental sites [30], [31]. [31] discussed circumstantial evidence pointing to a link between the non-closure of the energy balance with CO_2 fluxes while [30] mostly attributed the imbalances to miscalculations and scale issues, either in the available energy (net radiation or ground heat flux), or in the resulting turbulence measurements. Energy imbalance can also arise from advective fluxes and/or an inadequate sampling of low frequency turbulent motions [32]. Here, attempt is only made at correcting the terms in Equation (3). We nonetheless recognize the likely existence of other error sources to the SEB non-closure.

Corrections of the energy imbalance at the site

The lack of energy closure at the Verdu site was observed to mainly originate from the insufficient soil heat flux and the radiances measured by the net radiometer (i.e. the lack of representativeness of the radiance and soil heat flux measurements, which for practical reasons were mostly located over the vegetation). Errors in the soil heat flux often result from insufficient or missing calculations in the storage term, i.e. the heat stored in the soil above the heat plate [30]. The calorimetric method [33] was applied to account for the soil heat storage between the probe and the soil surface. The calorimetric approach is preferred in the majority of storage corrections since it has been documented as not being very sensitive to input data [34], [35]. Accordingly, the corrected hear storage is written as, $\mathrm{G_0} = \mathrm{G_{0-\delta Z}} + \mathrm{C}(\partial\mathrm{T}/\partial\mathrm{t})\delta\mathrm{Z}$; where $\mathrm{G_{0-\delta Z}}$ is the ground heat flux observed at a depth δZ below the ground surface, C [$\mathrm{J\,m^{-3}\,K^{-1}}$] is the volumetric heat capacity of the soil layer, which is calculated by weighting the heat capacities of the various soil components by volume [33], [34]. $\partial\mathrm{T}/\partial\mathrm{t}$ [$\mathrm{K\,s^{-1}}$] is the change in soil temperature (T) over time (t) and δZ [m] is the thickness of the soil layer, 5 cm here. The soil water content and soil temperature measurements were used in these calculations. Missing soil temperatures to be used in the corrections were reconstructed using a sinusoidal method that related existing surface soil temperature with available [5 cm] soil temperatures. A Savitzky-Golay filter [36] was applied to smooth out any sharp variations. Temperature has the greatest influence on $\mathrm{G_0}$ estimates [35] deeming these transformations for missing soil temperatures necessary. It is however acknowledged the reconstructions may have further contributed to the energy balance uncertainties.

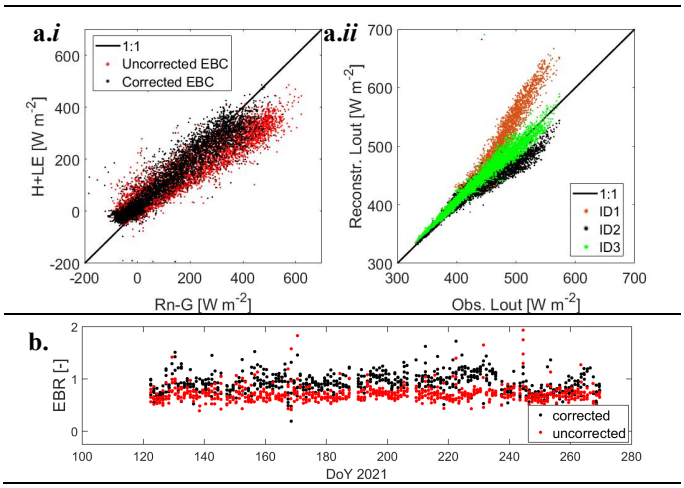

Figure 2: *a.i)* The energy balance closure in terms of the available energy and turbulent fluxes at the Verdu site; *a.ii)* the measured upwelling thermal emission compared to emissions calculated using the different component temperature

measurements; *b)* the uncorrected and corrected mid-day energy balance ratios (which is defined as the turbulent fluxes to available energy) over the period

The radiance measurements from the net radiometer also underwent some corrections. This was to reduce any scale biases emanating from the fact that the four-stream instrument was located just above the vegetation canopy. An initial comparison of the outgoing longwave radiation to the surface emission as calculated from the component temperatures (from the thermal sensors) showed that the measured longwave radiation was mostly coming from the exposed vegetation elements (ID3 in Figure 2a.*ii*). Following similar logic, the same issue could also be expected to influence the short wave radiance observations. Rescaling the radiations based on the relative fraction covers of the soil and vegetation resulted in a net radiation estimate that helped reduce the lack of energy closure.

Figure 2 illustrates the observed energy balance, both with and without flux corrections (specifically, Figure 2a.*i*, Figure 2b plot the [un]corrected energy balance closure). The energy closure error from the observed data was quite apparent, with only ~69% of the available energy being accounted for by the eddy-covariance measurements. The corrections made to the soil heat flux, i.e. by including the soil storage term of the top layer (using the calorimetric method), resulted in an improvement of the energy balance closure slope by ~1000 basis points to ~77 %. The shape – as described by the correlation coefficient – remained more or less the same, i.e., 0.95, 0.94 for the corrected and uncorrected cycles, respectively. This mostly affected the daytime exchanges, where – as expected – failure to include the top 5 cm soil layer led to significant underestimation of the storage term. A less trivial aspect is related to the scale/footprint of the radiation (thus available energy) versus the turbulent flux measurements. To further refine the closure, the net radiation was therefore reconstructed to address the potential scale issues arising from the proximal positioning of the net radiometer to the vegetation (see the outgoing longwave emission comparisons in Figure 2a.*ii* where radiation measurements generally tally with the exposed vegetation emissions). A further enhancement of the closure was henceforth achieved, with the regression slope improving to ~87.5%. The averaged daytime energy balance ratio ($EBR = (H + \lambda E)/(R_n - G_0)$, i.e., fraction of the daytime turbulent fluxes to the available energy) shows an improvement to 0.93 from 0.61, with a similar enhancement as the EBC slope. The mid-day EBR of the corrected energy balance terms (Figure 2b) is also closer to the 1-to-1 equivalence throughout the experimental period. The corrected fluxes were applied in the further evaluations of the surface energy balance modelling below.

Reconstructed directional temperature

The thermal cameras were installed to monitor the thermal infrared emission of the surface components throughout the experimental period. The field setup – with the relative positioning of the thermal sensors – is shown in **Figure 1**B. That is, two cameras (ID1 and ID3) observing the sunlit soil and vegetation elements and the ID2 camera observing the shaded vegetation. The shaded soil was not very apparent especially at the beginning of the growth cycle; as such, its temperature was retrieved as the cold pixels from the oblique looking cameras. Since the vineyard was kept at relatively similar/uniform conditions (in terms of irrigation and other practices), and given the logistical issues faced during set-up, we reasonably assumed that the temperatures observed at point scale were spatially representative of the entire site. Similarly, minimal mismatch between the EC and LST footprints could be assumed. Retrieval of emissions by source calls for emissivity correction of the observed brightness temperatures. Accordingly, we used the [manufacturer] recommended simple correction method (i.e., inversion of the Stefan Boltzmann equation) to obtain the component (or target) radiative temperatures (T_{xy}) from the thermal sensor observations,

$$T_{xy} = \left(\frac{T_{sensor}^4 - (1-\varepsilon)\varepsilon_{background} T_{background}^4}{\varepsilon} \right)^{0.25} \quad (4)$$

The air temperature served as the background temperature in these corrections. The emissivities of the soil and vegetation targets were taken as 0.96 and 0.98, respectively, while the atmosphere's apparent emissivity (emissivity of the background) was estimated using method in [37], [38]; i.e., $\varepsilon_{background} = \varepsilon_a = F\varepsilon_a^{cs}$; where $\varepsilon_a^{cs} = 1.24(e_a/T_a)^{1/7}$ is the clear sky apparent emissivity. e_a and T_a are the air vapour pressure and temperature, respectively. F is a parameterized factor that scales the clear-sky emissivity to cloudy conditions [38], [39]. Further correction for the sensing wave-band was done using expressions from [40] and [41].

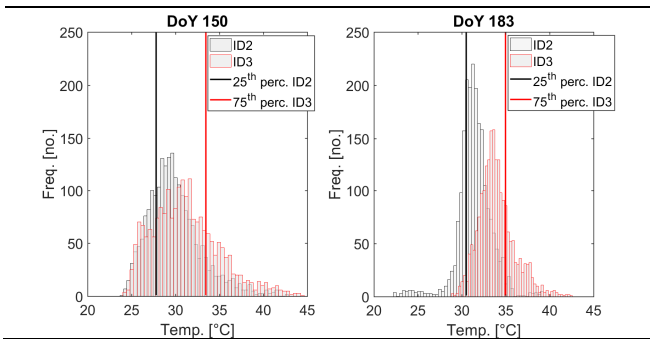

Figure 3: Overlaps of measurements from the ID2 and ID3 thermal cameras for DoYs 150 and 183

The directional surface temperature used to drive the models was subsequently reconstructed from the elemental temperatures weighted by their respective cover fractions in the view direction (both nadir and off-nadir). Due to the likelihood of mixed pixels, the sunlit elements were taken as the ~75th percentile of the observations from the cameras in the sun, while the shaded vegetation temperatures were taken as the ~25th percentile of the pixels in the TIR camera inclined to view the shaded vegetation elements. There are large overlaps between the shaded and sunlit cameras (e.g., ID2 and ID3, respectively, see Figure 3) and to discriminate the relative

extremes of the sunlit/shaded elements, the overlaps could be negated by using the bounds. The Chebyshev's inequality theorem, which is more general and can thus be applied to any probability distribution, yields $P(|T - \mu| \geq \sqrt{2}\sigma) \leq 50\%$ for the foremost realistic bound, $\mu \pm \sqrt{2}\sigma$; μ is the mean and σ the standard deviation. Accordingly, respective values at $\sim\mu - \sqrt{2}\sigma$ and $\sim\mu + \sqrt{2}\sigma$ were selected to represent the shaded and sunlit elements in place of the respective mean (μ) values. This was nonetheless somewhat arbitrary but realistic (notably when compared to the respective retrieved/modelled temperatures).

The weighting expression for the surface temperature is written thusly (e.g. [11]);

$$T_{\mathrm{surf}} = \left[\sum_{\mathrm{xy=vs,vh,gs,gh}} K_{\mathrm{xy}}(\theta_v, \varphi_v) T_{\mathrm{xy}}^4\right]^{0.25} \quad (5)$$

where $K_{\mathrm{xy=vs,vh,gs,gh}}(\theta_v, \varphi_v)$ are the fractions of the individual surface components computed from the canopy allometric features and sun-target-view geometry as described in the Unified François model [16], [17] (the RTM used within the extended SPARSE, and described in the previous sub-section), and T_{xy} are the elemental or component temperatures of the sunlit/shaded soil and vegetation. Subscripts xy denote the sunlit (s) and shaded (h) for x, and y denotes the soil (g) and vegetation (v) elements.

In UFR97, a turbid vine model, thus considering a discontinuous row canopy, is assumed while the vine mock-up in DART was more realistic (**Figure 1**B). Sunlit and shaded temperatures were then used as inputs of the UFR97 model, using the reconstruction expression (Equation (5)). In DART, the average soil and vegetation temperatures [$T_{ave}=(T_{sun} + T_{shd})/2$] were needed as input and a [$\Delta=(T_{sun} - T_{shd})/2$] used to assign illuminated [$T_{ill} = T_{ave} + \Delta$] and shaded [$T_{shd} = T_{ave} - \Delta$] mock-up element temperatures for the directional temperature simulations).

Input and methodology

The variables required to drive the surface energy balance schemes (SPARSE/SPARSE4) include: meteorological conditions (wind speed, air temperature and humidity), and the surface biophysical characteristics (leaf area index, vegetation height, etc.). **Table 1** below details these model inputs and the flux observations that are required when evaluating the SEB methods.

Boundary conditions are described by the surface temperature input (which in SEB modeling is often taken as the reconstructed directional LST from aggregated individual element (soil and vegetation) temperatures, and can thus aid in describing conditions/exchanges at the aerodynamic level), as well as the potential and stress limits mentioned earlier. The minimum stomatal resistance for the vineyard was taken from [42].

Table 1: Model inputs: summary of meteorological, biophysical and flux information

Data	*Source* [Range]
Model inputs (for both SPARSE and SPARSE4)	
Bio-physical parameters: Leaf area index (LAI – [$m^2 m^{-2}$])	*Field* [varying]
Leaf inclination distribution function (LIDF [-])	*Literature* [spherical assumed - $\mathcal{G}$ = 0.5]
Vegetation height [m]	*Field* [varying]
Minimum stomatal resistance (r_{stmin} - [$s\ m^{-1}$])	*Literature* [100 s/m]
Atmospheric forcing and observed turbulent fluxes	
Meteorological data: Incoming solar radiation ([$W\ m^{-2}$]), air & surface temperature [°C], relative humidity [-], wind speed [$m\ s^{-1}$]	*Field* [varying - ***Figure 1**.C*]
Fluxes [$W\ m^{-2}$]: radiation; latent, sensible and ground heat	*Field* [varying]
Other data	
Viewing direction: Zenith *(SPARSE and SPARSE4)* and Azimuth *(SPARSE4)*	*Field* [nadir and oblique VZA = ∼0 − 60; VAA = ∼0 − 360]
Solar direction [°]: Zenith and Azimuth *(SPARSE4)*	*from local time & geo. co-ord.* [solar algorithm]

The processed temperature data (i.e. emissivity corrected thermal measurements) were first used as input in radiative transfer schemes to perform an inter-comparison exercise. Three clear-sky days (DoYs: 128, 183, 211) were selected to perform these experiments. Consequently, directional surface temperatures simulated by the UFR97 [16] and the 4SAIL [21] radiative models were evaluated against those simulated by the 3D DART [20] radiative scheme, taken as the 'reference', using 3D vine objects/mock-ups that were created with the blender.org software and pictures of vines.

The reconstructions of directional temperatures as applied in the experiments are described above. The surface energy balance methods (SPARSE and SPARSE4) were then driven using these reconstructed surface temperatures. In the first part, the surface temperatures of the entire campaign period were used and the models evaluated using the EB EC observations. The second part involved the evaluation of the SEB schemes in terms of directionality. The evaluations of the SPARSE and SPARSE4 models (in directional consistency experiments) using the reconstructed directional surface temperatures were

separately based on: *i)* reconstructions by UFR97 over the whole period, and *ii)* reconstructions from DART over the selected clear sky days.

III. Results

A. Temperature reconstructions: surface temperature comparison - simple RTMs for complex canopy architectures

In this section, we propose to evaluate the UFR97 radiative transfer model [16], [18] by comparing it with DART [20], as well as 4SAIL [21]. Accordingly, we compare surface temperatures simulated by the different RTMs. The UFR97 radiative transfer method has already been evaluated against the thermal radiosity-graphics combined model, a 3D radiative transfer method, where its retrieval capabilities were demonstrated over continuous as well as heterogeneous (row and forest) canopies [16]. In their work, UFR97 was observed to outperform 4SAIL over heterogeneous/non-continuous canopies. Those evaluations are thus complemented here by the use of the 3-D DART model for 3 selected clear-sky days. DART has been cross-validated within the Radiation Transfer Model Intercomparison (RAMI) exercises [43], [44] and in TIR experiments [45], where it has been shown to provide realistic and accurate radiative components over homogeneous and heterogeneous canopies. The data used for this exercise has been described above.

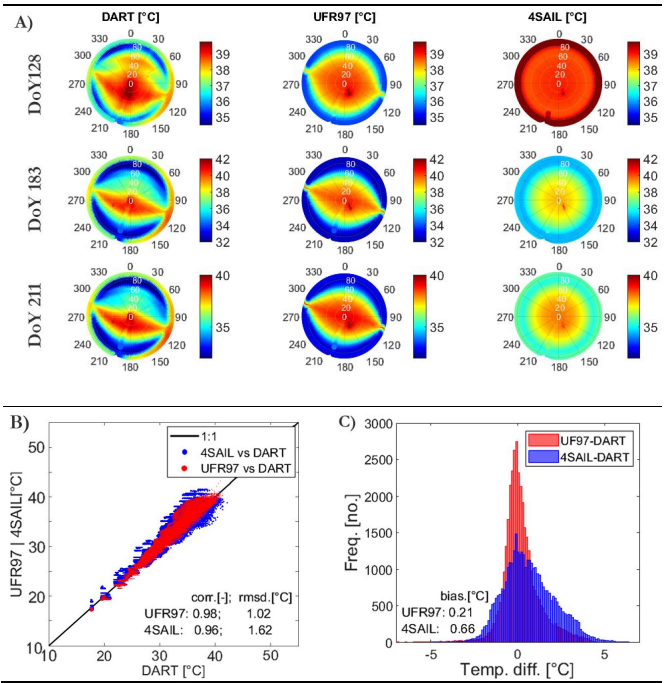

Figure 4: Inter-comparison of the UFR97 (and 4SAIL) temperatures to those simulated by the DART 3-D radiative transfer model. A) noon polar plots depicting the simulated angular temperatures; presented separately for the 3 selected periods (noon solar angles [*DoY* SZA SAA]: [*128* 25.17° 147.67°]; [*183* 19.46° 139.49°] ; [*211* 23.89° 140.96°]) B) scatterplots and metrics of day-time UFR97 and 4SAIL-retrieved surface temperatures versus those simulated by the 3-D DART model, and C) the corresponding histograms of temperature differences. B) and C) combine all daytime data.

Considering that DART simulations utilized realistic vine mock-ups (see **Figure 1**B), the UFR97 model (which relies on a turbid geometrical model) performs quite well when retrieving the directional signals, and generally outperforms the 4SAIL radiative method that is classically based on a homogeneous canopy. As such, the row geometry consideration in UFR97 ensures better realism of the simulated directional temperatures, especially along the row (see Figure 4). The distribution of differences (Figure 4C) also shows that the UFR97-estimated temperatures were generally close to those simulated by DART, yielding a mean error of 0.21 °C versus 0.69 °C achieved by the 4SAIL radiative transfer.

B. Model estimates

To simulate the energy budget components, the SPARSE/SPARSE4 energy balance modelling schemes were first forced using the reconstructed nadir surface temperatures (in addition to other meteorological inputs) - Equation (5). Figure 5 scatters the estimated turbulent fluxes against the observations. As exhibited by the daylong performance metrics, the models satisfactorily (and similarly) retrieved the overall fluxes. There was however a tendency for the models to overestimate the daytime sensible heat flux while somewhat underestimating the respective nighttime flux at the site leading to relatively small biases (overall biases for SPARSE and SPARSE4 were -5 W m^{-2} and -3 W m^{-2}, respectively). In addition to inherent model-induced errors, this could also in part be attributed to measurement errors as given by the observed energy imbalance, i.e., lower observed turbulent fluxes relative to the measured available energy. While the representation of the surface as a row-scene helps in the realistic characterization of flux partitioning, this does not necessarily translate into a significant improvement in overall performance. Generally, the two SEB schemes do not show significant differences when simulating the overall fluxes, especially when forced using nadir surface temperatures. This can perhaps be explained by the fact that both methods use a relatively identical model structure, with similar physical/theoretical basing, such as the representation of turbulence (i.e., aerodynamic exchanges/interactions between the surface and the atmosphere). Provided the correct effective canopy area together with surface temperatures with minimal thermal directionality influences are used in surface energy modelling, reasonable flux retrievals can seemingly be achieved.

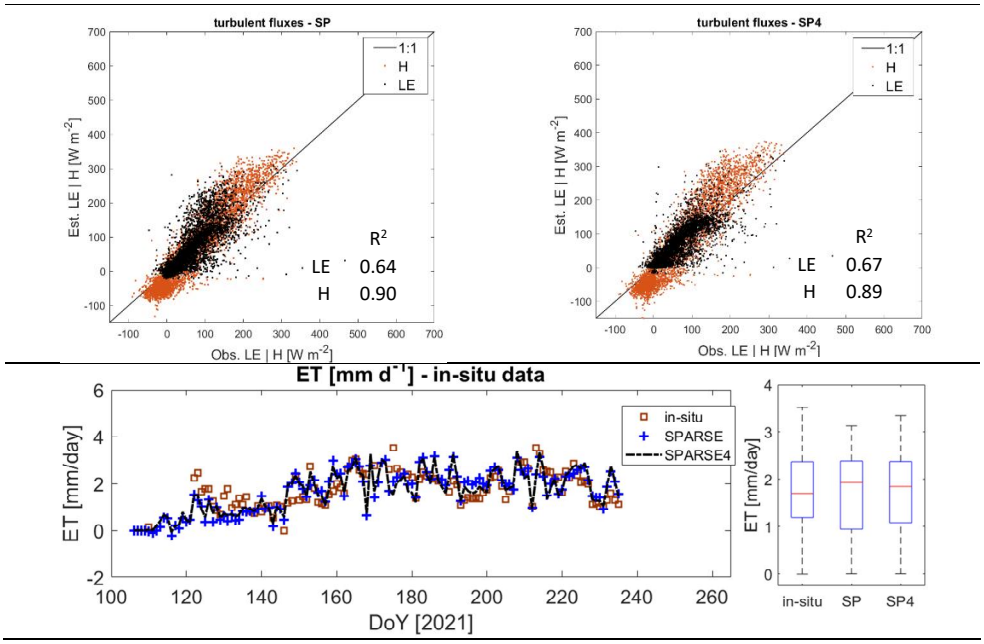

Figure 5: *top)* scatter plots of simulated versus observed turbulent fluxes at the Verdu site; left, SPARSE and right, SPARSE4; *bottom)* modelled (using in-situ meteorological and ancillary data) and in-situ daily evapotranspiration time-series'

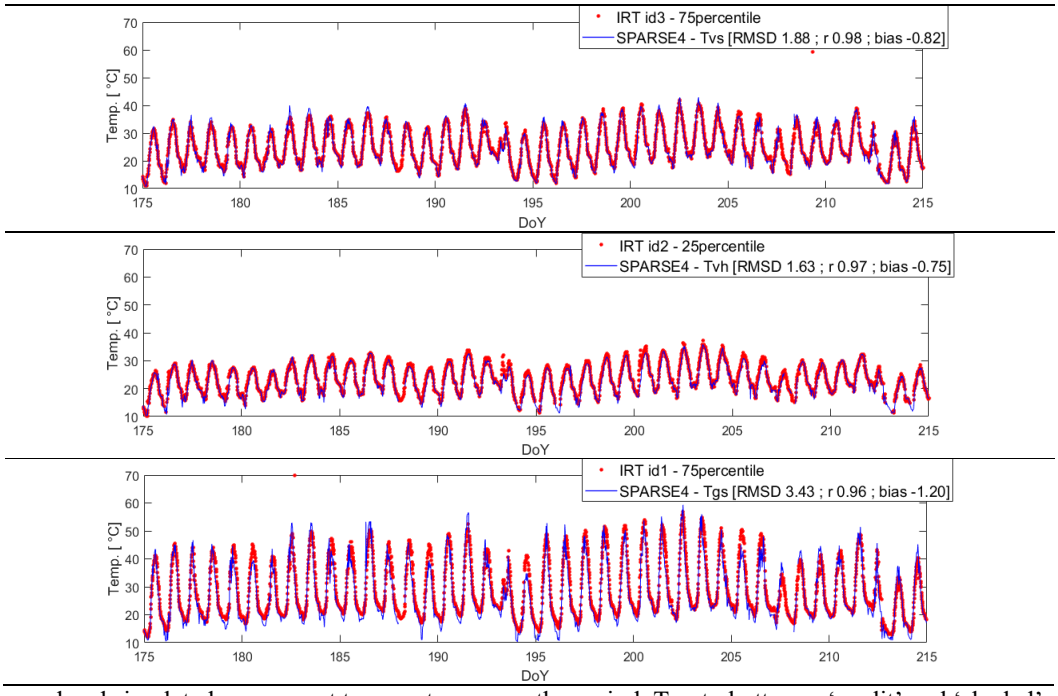

Figure 6: Observed and simulated component temperatures over the period. Top to bottom – 'sunlit' and 'shaded' vegetation and 'sunlit' soil, respectively

Separately, the surface energy balance models also simulated source temperatures, which could hence be compared with the observations. Overall, the estimated component temperatures were realistically reproduced. Qualitatively, this is illustrated in the time series' in Figure 6 - i.e. the thermal camera measurements (labelled *ID1*, *ID2*, *ID3* in **Figure 1**B) and the modelled temperature. Quantitatively, these modelled temperatures were satisfactory (**Table 2**). The coefficients from the UFR97 were used in weighting of the elemental temperatures for the average component temperatures used in the performance metrics calculations in **Table 2**

Table 2: Performance metrics of the overall fluxes and recalculated* average component temperatures

	SPARSE			*SPARSE4*		
	RMSD	*r*	*bias*	*RMSD*	*r*	*bias*
	[W m^{-2}]	*[-]*	*[W m^{-2}]*	*[W m^{-2}]*	*[-]*	*[W m^{-2}]*
LE	39	0.80	3	37	0.82	2
H	50	0.95	-5	52	0.94	-3
G	49	0.78	17	49	0.77	11
Rn	32	0.99	14	33	0.99	15
	[K]	*[-]*	*[K]*	*[K]*	*[-]*	*[K]*
T_v^*	3.14	0.95	-0.49	1.65	0.98	-0.77
T_g^*	3.65	0.95	-0.58	3.15	0.96	-1.13

C. Directional consistency: quasi-synthetic analyses

Ideally, the estimated surface fluxes should exhibit overall satisfactory consistency, irrespective of the viewing direction of the thermal signal input. That is, they should not be affected by the sensing direction/geometry of a remote sensor. To check this retrieval consistency, the directional surface temperatures were reconstructed using Equation (5) as detailed in the methods section above. These were then used to rerun the models for comparison of the oblique-retrieved fluxes versus the nadir-retrieved ones. The polar plots of the resulting metrics (in terms of the Mean Absolute Error and the relative Root Mean Square Difference) are illustrated in **Figure 7** (separately, the plots derived from using DART temperature data are shown in **Figure 8**). $\mathrm{MAE} = \frac{1}{n}\sum_{i=1}^{n}\left|\mathrm{X}_{\mathrm{dir},i} - \mathrm{X}_{\mathrm{ref},i}\right|$ and $\mathrm{rRMSD} = \frac{\sqrt{\frac{1}{n}\sum_{i=1}^{n}\left(\mathrm{X}_{\mathrm{dir},i}-\mathrm{X}_{\mathrm{ref},i}\right)^2}}{\overline{\mathrm{X}_{\mathrm{ref}}}}$; where $\mathrm{X}_{\mathrm{dir}}$ and $\mathrm{X}_{\mathrm{ref}}$ are the directional-retrieval and reference (nadir-based or observation) variables (latent and sensible heat energy fluxes), respectively.

Retrieval consistency is generally degraded cross-row with a much better consistency between nadir and oblique retrievals along the vine row. Along row, the gap fraction tends to remain relatively constant from nadir to higher zenith angles. This is however not the case cross-row where the observed vegetation fraction cover will increase with decrease in elevation. Early on in the growth period, when the surface is mostly bare, thermal directionality effects are mainly observed to influence flux retrievals in the hotspot region (**Figure 7** a). For such periods, the influences are nonetheless small. Even for periods with relatively full row development, the hotspot region somewhat adds to the nadir versus oblique flux retrieval inconsistencies. The row geometry's contribution to the retrieval directionality influences also becomes apparent during this growth stage (especially at larger zenith angles). This is indeed observed for both SEB schemes with varying magnitudes, but more pronounced in SPARSE most likely due to its canopy homogeneity assumption.

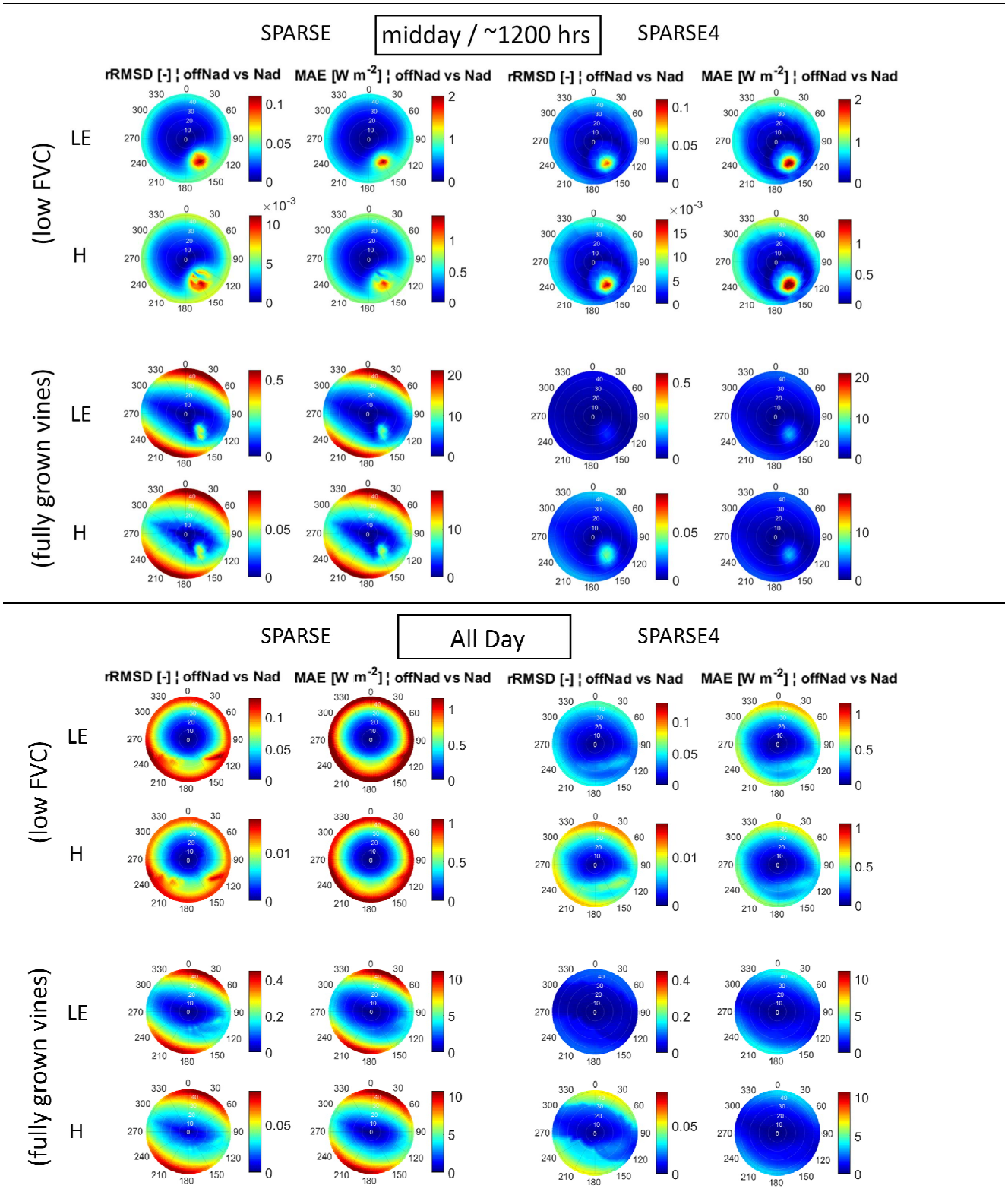

Figure 7: LE and H polar plots of oblique-vs-nadir rRMSD and MAE for the growth period – i.e., periods with low vegetation cover and with fully grown vines [noon and all-day]

1

In addition to the full period dataset that contained the directional temperatures reconstructed using the UFR97 model (as described above, i.e. Equation (5)), the sample dataset used for the DART comparisons was also applied to the models. This

data was limited to only three clear-sky days. A comparison of the directional temperature reconstructions to those simulated by the 3D DART model (as used hereafter) are illustrated in Figure 4. Figure 8 below shows the directional inconsistencies observed when the DART temperatures were used in the inversion of the surface energy balance (latent and sensible energy fluxes) in SPARSE and SPARSE4. The polar plots depict the relative-RMSD (left) and mean absolute error (right) of oblique-based versus nadir-based flux retrieval estimates. Two top rows in Figure 8 - for the consistency evaluations; and two bottom rows - the retrievals based on directional surface temperatures but compared to the respective EC observations.

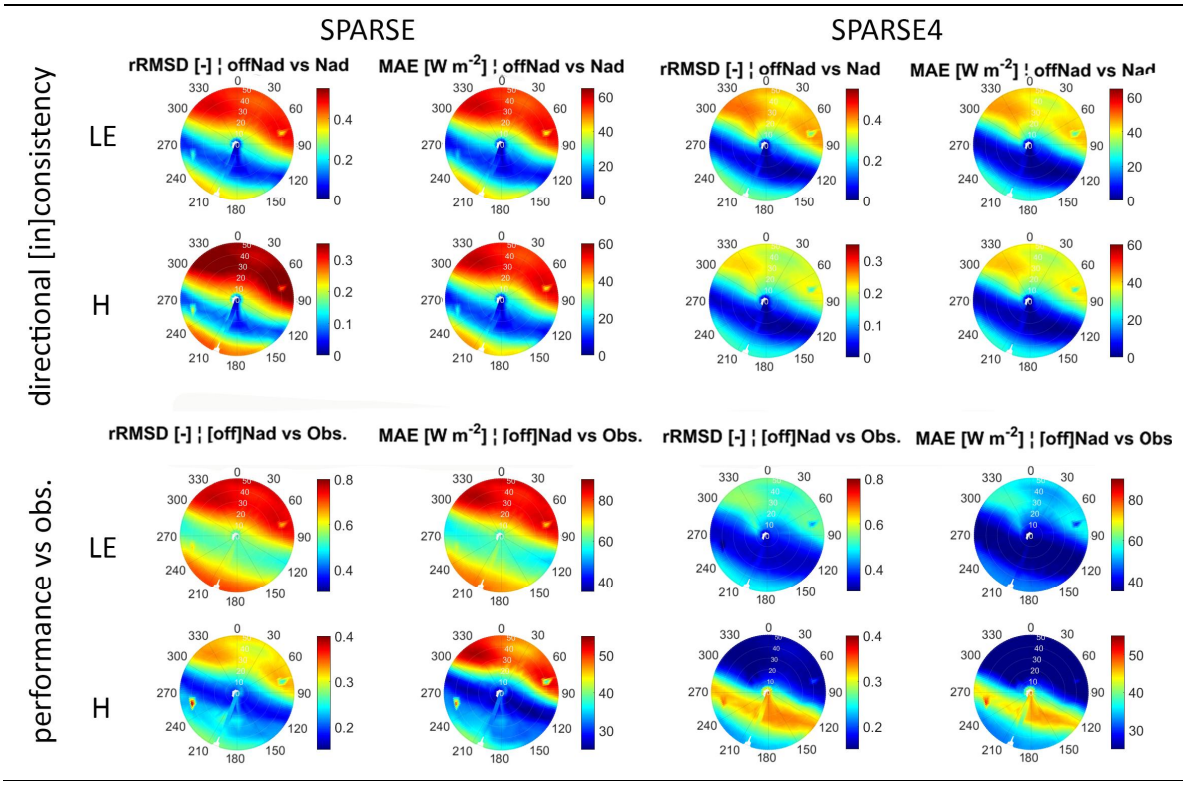

Figure 8: directional inconsistency (nadir- versus oblique-based estimates) for the two SPARSE surface energy balance methods; b) comparison of the directional retrievals as compared to the eddy covariance observations. Polar plot illustrations use the around noon data over the three selected clear-sky days

IV. Discussion

A. Implication of applying simple RTMs for complex canopy architectures

The consideration of the row architecture in UFR97 ensures that the distribution of temperatures over the angular viewing space (that is, shape of polar plots, particularly along the rows) is rather well reproduced, in comparison to the DART model. This is an important aspect especially when considering the inversion of (directional) brightness temperatures for turbulent fluxes in energy balance modeling. Relatively simple SEB methods can benefit from such radiative transfer realism when estimating and partitioning energy/water fluxes over heterogeneous (row) canopies.

It however appeared that a turbid model such as the unified François model could not model some specific phenomena. For example, the column used to represent the row (where the canopy leaf area is uniformly grouped vertically - see illustration in **Figure 1**.B, in green) may not be very realistic given that a vine generally consists of the lower part (trunk) and the upper whorl structure (see **Figure 1**). At relatively low sun elevation, such a complex canopy structure makes it possible to observe more shadows (or vice versa) especially when viewing from low elevation angles. The symmetry of the UFR97 tends to disperse the simulations uniformly across the row. This arises from the fundamental description of the method, i.e., it is essentially a product of the gap probability (based on the row geometry [18]) and the anisotropy variations of illuminated / shaded probabilities of [46] that are based on a homogeneous scene, and also the illumination modifications made in [16]. A better representation of the row shape, for example the enhancement described in [47], could perhaps provide a more detailed radiative transfer modelling with improved realism.

B. Retrieval sensitivity to thermal directionality

Modelling surface exchanges using directional remotely-sensed surface temperature data requires that the applied SEB methods exhibit little sensitivity to such angular inputs. Ideally, TRD-influenced surface brightness temperatures should consistently describe the prevailing terrestrial water status conditions – in both observation and simulation setups. In the latter, such an optimal outcome is unlikely to be achieved due to physically deficient

methods that have to rely on and model several related/interdependent and interacting variables and processes. As observed in the current study, canopy structure and landscape heterogeneity are some of the surface characteristics that are often inexactly represented in modelling schemes.

By incorporating the UFR97 radiative transfer scheme that supports heterogeneous [in addition to homogeneous] landscapes, SPARSE4 is able to better ensure consistency of modelled surface exchanges when driven with directional surface temperature, especially at cross-row higher zenith angles.

Notwithstanding the heterogeneity offered, the application of simple radiative models to represent complex canopies is not without limitation, as is shown in the current work. The symmetry (in the simple turbid models: here the heterogeneous UFR97 and homogeneous [19] / Beer Lambert's schemes) versus the dissymmetry (in DART with the more realistically modelled vine mock-up) in the simulated directional temperatures described above does indeed influence the retrieval consistency between different thermal infrared input directions. Along the row (i.e., at view angles close to the row direction), DART simulates relatively contrasting temperatures in the directions in and away from the Sun's direction. While the symmetric simulations by the UFR97 model in the Sun's direction can reproduce the temperature distributions in DART, the lower temperatures close to the row - in the direction away from the sun - are not well mimicked. As pointed out earlier, this could perhaps be ascribed to the radiative method applied, which is a product of row gap frequency according [18] and the illumination/shade anisotropy variations or probabilities of [46] that are based on a homogeneous scene. Applying such disparately lower temperatures when inverting the surface energy balance tends to infer a lower surface water-stress. Henceforth, the lower temperatures in the Sun's opposite direction are inconsistently manifested in the form of higher [lower] latent [sensible] heat fluxes.

Better directional consistency does not necessarily imply an overall better model performance. Whereas the oblique-based (close to zenith) model estimates can be seen to be consistent with the nadir-based estimates (with degraded consistency further off-nadir), the performance relative to the true or real observations may indicate and thus be interpreted otherwise. Unless the inconsistencies manifest in large magnitudes (as would be the case in scenes with moderate-to-large vegetation fraction covers), then standardizing / normalizing the directional thermal data to a specific direction (for instance, nadir) should not be assumed to result in better flux estimations. As shown in Figure 8 (i.e., sensible heat flux estimated using SPARSE4), the performance further off-nadir can sometimes be better than the more consistent near-nadir estimates. Nonetheless, more robust algorithms that ensure directional consistency are necessary as that would give users confidence in obtaining appropriate direction-independent outputs.

V. Summary and Conclusion

An experimental field study was carried out in the framework of HiLiaise project aiming at monitoring surface energy balance components of a vineyard in Verdu, Catalonia, Spain. The processed and corrected (for the observed energy imbalance) fluxes are presented. The energy balance closure was improved considerably after correcting the available energy (net radiation - soil heat flux) terms. That is, by including the top layer storage term for the overall soil heat flux and the enhancement of the radiances measured by the net radiometer to account for scale (or proximity) issues. These measurements were then applied for onward assessment of methods used to estimate the surface energy balance. For the surface energy balance modelling, the directional surface temperature was initially reconstructed from the measured elemental temperatures whereupon we demonstrated the applicability of the relatively simple Unified François model over the heterogeneous row canopy. While homogeneity of the surface is often assumed in methods used for characterizing land surface processes, it is necessary to consider realistic canopy geometries for better modelling of angular anisotropy dynamics. A preliminary comparison between the UFR97 model, 4SAIL and the 'reference' DART simulations was thus performed, where it was shown that the UFR97 simulations were more consistent with the DART 'truths' particularly in terms of temperature distribution over the polar space.

From runs using the nadir-reconstructed surface temperatures, the surface energy balance SPARSE schemes yielded reasonable surface turbulent flux estimates, which as somewhat expected were relatively similar since both methods are based on a similar model structure (model assumptions, physics, among others). A realistic retrieval of component thermal emissions was also achieved where the overall trends and magnitudes of the various surface elements were replicated. To check the angular retrieval consistency, the reconstructed temperatures (directional, i.e. nadir and off-nadir) were used to re-run the SPARSE and SPARSE4 energy balance schemes. Both methods ensured flux consistency along-row with degraded performance being observed cross-row. This was more pronounced in the SPARSE estimates, which could be attributed to the inherent continuous/homogeneous surface assumption.

The study has demonstrated the necessity of incorporating more realistic canopy representations if directional retrieval consistency is to be maintained. While the use of a homogeneous radiative scheme may be sufficient when using near-nadir thermal measurements, improved modelling of the canopy should allow better flux consistency especially for higher view angles. However, the realism of simple radiative schemes used for heterogeneous surfaces needs to be improved to mimic naturally occurring asymmetries (as modelled by more complex 3D models) and thus reduce directional effects. The asymmetry in directional data from the more realistic 3D DART model showed that there is a real need for a better representation of the turbid models used in the radiative scheme. This could possibly involve, *inter alia*: better description of the row shape and structure (as introduced in [47]), which should include representing the vertical vegetation column (especially of tree canopies) with better realism (for instance, considering the upper whorl and lower trunk separately for realistic directional gap frequency estimations); considering other leaf distributions (inclinations and orientations) that also occur in natural terrestrial systems, such as planophile / erectophile leaf distributions. Since such considerations would require collection of additional biophysical-related data, care should be taken to ensure a

parsimonious modelling principle. Regarding accounting for directional effects in single-source RS-based SEB methods, where homogeneous canopies are often assumed, there is need to formulate simple kernel-driven radiative schemes for heterogeneous (e.g. row) structures to aid in the inversion for surface fluxes over such canopies.

Given the specificities in the current study (that is, the unique setup and heterogeneity at the experimental site), we acknowledge that the results should generally be interpreted in the context of local or point-scale surface exchange observation and modelling. Over large spatial scales, the surface (as depicted in satellite pixels) is likely to be composed of mixed canopies. The aforementioned schemes (especially those that are based on mixed-pixels, such as the framework proposed in [9] and the angular normalization method applied on MODIS LST data by [48]) could perhaps be better suited for low resolution application purposes, thus warranting further analyses and refinement of such methods.

ACKNOWLEDGMENT

This work was supported by the ALTOS project (PRIMA 2018 - Section 2), with grants provided by ANR via the agreement n°ANR-18-PRIM-0011-02 as well as the CNES/TOSCA program for the TRISHNA project. First author acknowledges the financial support of his PhD from CNES and Région Occitanie. The field experiments were carried out in the context of the HiLiaise and ESA WineEO projects. Joan Boldu (proprietor) and David Tous (SafSampling) are also acknowledged for allowing/providing access to the site and other site related data. Nicolas Lauret's help with preparation of the DART mock-ups is appreciated.

REFERENCES

[1] G. S. Campbell and J. M. Norman, *An Introduction to Environmental Biophysics*, 2nd ed., vol. 6, no. 4. New York, NY: Springer New York, 1998.

[2] Z. Su, "The Surface Energy Balance System (SEBS) for estimation of turbulent heat fluxes," *Hydrol. Earth Syst. Sci.*, vol. 6, no. 1, pp. 85–100, Jun. 2002.

[3] W. G. M. Bastiaanssen, M. Menenti, R. A. Feddes, and A. A. M. Holtslag, "A remote sensing surface energy balance algorithm for land (SEBAL). 1. Formulation," *J. Hydrol.*, vol. 212–213, no. 1–4, pp. 198–212, Dec. 1998.

[4] J. M. Norman, W. P. Kustas, and K. S. Humes, "Source approach for estimating soil and vegetation energy fluxes in observations of directional radiometric surface temperature," *Agric. For. Meteorol.*, vol. 77, no. 3–4, pp. 263–293, 1995.

[5] N. Farhani, J. Carreau, Z. Kassouk, M. Le Page, Z. Lili Chabaane, and G. Boulet, "Analysis of Multispectral Drought Indices in Central Tunisia," *Remote Sens.*, vol. 14, no. 8, p. 1813, Apr. 2022.

[6] G. Boulet, A. Chehbouni, P. Gentine, B. Duchemin, J. Ezzahar, and R. Hadria, "Monitoring water stress using time series of observed to unstressed surface temperature difference," *Agric. For. Meteorol.*, vol. 146, no. 3–4, pp. 159–172, 2007.

[7] B. Cao *et al.*, "A review of earth surface thermal radiation directionality observing and modeling: Historical development, current status and perspectives," *Remote Sens. Environ.*, vol. 232, no. October 2018, p. 111304, 2019.

[8] K. Tha Paw U, "Development of models for thermal infrared radiation above and within plant canopies," *ISPRS J. Photogramm. Remote Sens.*, vol. 47, no. 2–3, pp. 189–203, Apr. 1992.

[9] Y. Jiang, R. Tang, and Z.-L. Li, "A framework of correcting the angular effect of land surface temperature on evapotranspiration estimation in single-source energy balance models," *Remote Sens. Environ.*, vol. 283, p. 113306, 2022.

[10] A. Olioso *et al.*, "Evapotranspiration mapping from remote sensing data: uncertainties and ensemble estimates based on multimodel – multidata simulations," in *International Workshop on High-Resolution Thermal EO, Turin, Italy*, 2023.

[11] J. P. Lagouarde, S. Dayau, P. Moreau, and D. Guyon, "Directional anisotropy of brightness surface temperature over vineyards: Case study over the Medoc Region (SW France)," *IEEE Geosci. Remote Sens. Lett.*, vol. 11, no. 2, pp. 574–578, Feb. 2014.

[12] T. N. Carlson, O. Taconet, A. Vidal, R. R. Gillies, A. Olioso, and K. Humes, "An overview of the workshop on thermal remote sensing held at La Londe les Maures, France, September 20–24, 1993," *Remote Sens. Rev.*, vol. 12, no. 3–4, pp. 147–158, Jan. 1995.

[13] M. A. A. Friedl, "Forward and inverse modeling of land surface energy balance using surface temperature measurements," *Remote Sens. Environ.*, vol. 79, no. 2–3, pp. 344–354, Feb. 2002.

[14] D. S. Kimes and J. A. Kirchner, "Directional radiometric measurements of row-crop temperatures," *Int. J. Remote Sens.*, vol. 4, no. 2, pp. 299–311, Jan. 1983.

[15] J.-P. Lagouarde *et al.*, "Indo-French High-Resolution Thermal Infrared Space Mission for Earth Natural Resources Assessment and Monitoring – Concept and Definition of Trishna," *ISPRS - Int. Arch. Photogramm. Remote Sens. Spat. Inf. Sci.*, vol. XLII-3/W6, no. February, pp. 403–407, 2019.

[16] Z. Bian *et al.*, "An analytical four-component directional brightness temperature model for crop and forest canopies," *Remote Sens. Environ.*, vol. 209, no. March, pp. 731–746, May 2018.

[17] C. Francois, C. Ottle, and L. Prevot, "Analytical parameterization of canopy directional emissivity and directional radiance in the thermal infrared. Application on the retrieval of soil and foliage temperatures using two directional measurements," *Int. J. Remote Sens.*, vol. 18, no. 12, pp. 2587–2621, 1997.

[18] B. Y. Yan, X. R. Xu, and W. J. Fan, "A unified canopy bidirectional reflectance (BRDF) model for row crops," *Sci. China Earth Sci.*, vol. 55, no. 5, pp. 824–836, 2012.

[19] T. Nilson, "A theoretical analysis of the frequency of

gaps in plant stands," *Agric. Meteorol.*, vol. 8, no. 1966, pp. 25–38, Jan. 1971.

[20] J. Gastellu-Etchegorry, "Modeling radiative transfer in heterogeneous 3-D vegetation canopies," *Remote Sens. Environ.*, vol. 58, no. 2, pp. 131–156, Nov. 1996.

[21] W. Verhoef, L. Jia, Q. Xiao, and Z. Su, "Unified optical-thermal four-stream radiative transfer theory for homogeneous vegetation canopies," *IEEE Trans. Geosci. Remote Sens.*, vol. 45, no. 6, pp. 1808–1822, 2007.

[22] G. Boulet *et al.*, "The SPARSE model for the prediction of water stress and evapotranspiration components from thermal infra-red data and its evaluation over irrigated and rainfed wheat," *Hydrol. Earth Syst. Sci.*, vol. 19, no. 11, pp. 4653–4672, Nov. 2015.

[23] S. Mwangi, G. Boulet, and A. Olioso, "Assessment of an extended SPARSE model for estimating evapotranspiration from directional thermal infrared data," *Agric. For. Meteorol.*, vol. 317, no. February, p. 108882, 2022.

[24] W. J. Shuttleworth and R. J. Gurney, "The theoretical relationship between foliage temperature and canopy resistance in sparse crops," *Q. J. R. Meteorol. Soc.*, vol. 116, no. 492, pp. 497–519, 1990.

[25] L. E. Street, G. R. Shaver, M. Williams, and M. T. Van Wijk, "What is the relationship between changes in canopy leaf area and changes in photosynthetic CO2 flux in arctic ecosystems?," *J. Ecol.*, vol. 95, no. 1, pp. 139–150, 2007.

[26] Y. Jiang, R. Tang, and Z.-L. Li, "A physical full-factorial scheme for gap-filling of eddy covariance measurements of daytime evapotranspiration," *Agric. For. Meteorol.*, vol. 323, p. 109087, 2022.

[27] A. J. McElrone, T. M. Shapland, A. Calderon, L. Fitzmaurice, K. T. Paw U, and R. L. Snyder, "Surface Renewal: An Advanced Micrometeorological Method for Measuring and Processing Field-Scale Energy Flux Density Data," *J. Vis. Exp.*, no. 82, Dec. 2013.

[28] R. Rosa and J. Tanny, "Surface renewal and eddy covariance measurements of sensible and latent heat fluxes of cotton during two growing seasons," *Biosyst. Eng.*, vol. 136, pp. 149–161, 2015.

[29] X. Zhao, Y. Liu, H. Tanaka, and T. Hiyama, "A Comparison of Flux Variance and Surface Renewal Methods With Eddy Covariance," *IEEE J. Sel. Top. Appl. Earth Obs. Remote Sens.*, vol. 3, no. 3, pp. 345–350, Sep. 2010.

[30] T. Foken, "The energy balance closure problem: An overview," *Ecol. Appl.*, vol. 18, no. 6, pp. 1351–1367, Sep. 2008.

[31] K. Wilson *et al.*, "Energy balance closure at FLUXNET sites," *Agric. For. Meteorol.*, vol. 113, no. 1–4, pp. 223–243, Dec. 2002.

[32] G. Wohlfahrt and P. Widmoser, "Can an energy balance model provide additional constraints on how to close the energy imbalance?," *Agric. For. Meteorol.*, vol. 169, pp. 85–91, 2013.

[33] T. J. Sauer and R. Horton, "Soil heat flux," *Micrometeorology Agric. Syst.*, no. 47, pp. 131–154, 2015.

[34] P. D. Colaizzi, S. R. Evett, N. Agam, R. C. Schwartz, and W. P. Kustas, "Soil heat flux calculation for sunlit and shaded surfaces under row crops: 1. Model development and sensitivity analysis," *Agric. For. Meteorol.*, vol. 216, pp. 115–128, 2016.

[35] C. Liebethal, B. Huwe, and T. Foken, "Sensitivity analysis for two ground heat flux calculation approaches," *Agric. For. Meteorol.*, vol. 132, no. 3–4, pp. 253–262, Oct. 2005.

[36] A. Savitzky and M. J. E. Golay, "Smoothing and Differentiation of Data by Simplified Least Squares Procedures," *Anal. Chem.*, vol. 36, no. 8, pp. 1627–1639, 1964.

[37] W. Brutsaert, "On a derivable formula for long-wave radiation from clear skies," *Water Resour. Res.*, vol. 11, no. 5, pp. 742–744, Oct. 1975.

[38] W. Brutsaert, *Evaporation into the Atmosphere*. Dordrecht: Springer Netherlands, 1982.

[39] J. Herrero and M. J. Polo, "Parameterization of atmospheric longwave emissivity in a mountainous site for all sky conditions," *Hydrol. Earth Syst. Sci.*, vol. 16, no. 9, pp. 3139–3147, 2012.

[40] S. B. Idso, "A set of equations for full spectrum and 8- to 14-μm and 10.5- to 12.5-μm thermal radiation from cloudless skies," *Water Resour. Res.*, vol. 17, no. 2, pp. 295–304, Apr. 1981.

[41] A. Olioso, "Estimating the difference between brightness and surface temperatures for a vegetal canopy," *Agric. For. Meteorol.*, vol. 72, no. 3–4, pp. 237–242, 1995.

[42] A. H. de C. Teixeira, W. G. M. Bastiaanssen, and L. H. Bassoi, "Crop water parameters of irrigated wine and table grapes to support water productivity analysis in the São Francisco river basin, Brazil," *Agric. Water Manag.*, vol. 94, no. 1–3, pp. 31–42, Dec. 2007.

[43] J. L. Widlowski *et al.*, "Third Radiation Transfer Model Intercomparison (RAMI) exercise: Documenting progress in canopy reflectance models," *J. Geophys. Res. Atmos.*, vol. 112, no. 9, pp. 1–28, 2007.

[44] B. Pinty *et al.*, "Radiation transfer model intercomparison (RAMI) exercise," *J. Geophys. Res. Atmos.*, vol. 106, no. D11, pp. 11937–11956, 2001.

[45] P. Guillevic, J. P. Gastellu-Etchegorry, J. Demarty, and L. Prévot, "Thermal infrared radiative transfer within three-dimensional vegetation covers," *J. Geophys. Res. Atmos.*, vol. 108, no. 8, pp. 1–13, 2003.

[46] A. Kuusk, "The hot-spot effect of a uniform vegetative cover," *Sov. J. Remote Sens.*, no. January, 1985.

[47] Y. Du *et al.*, "Modeling Directional Brightness Temperature (DBT) over Crop Canopy with Effects of Intra-Row Heterogeneity," *Remote Sens.*, vol. 12, no. 17, p. 2667, Aug. 2020.

[48] J. Wang, R. Tang, Y. Jiang, M. Liu, and Z. L. Li, "A practical method for angular normalization of global MODIS land surface temperature over vegetated

surfaces," *ISPRS J. Photogramm. Remote Sens.*, vol. 199, no. March, pp. 289–304, 2023.